3D Coupled Cellular Automaton (CA)-Finite Element (FE) Modeling for Solidification Grain Structures in Gas Tungsten Arc Welding (GTAW)

Shijia Chen, Gildas Guillemot, Charles-André Gandin

ISIJ International, Vol. 54 (2014), No. 2, pp. 401–407

3D Coupled Cellular Automaton (CA)–Finite Element (FE) Modeling for Solidification Grain Structures in Gas Tungsten Arc Welding (GTAW)

Shijia CHEN,* Gildas GUILLEMOT and Charles-André GANDIN

MINES ParisTech, CEMEF UMR CNRS 7635, 06904 Sophia Antipolis, France.

(*Received on August 26, 2013; accepted on November 5, 2013*)

A coupled Cellular Automaton (CA) – Finite Element (FE) model is proposed to predict the grain structure formation during Gas Tungsten Arc Welding (GTAW). The FE model solves the heat flow problem based on an adaptive meshing. This is done on a first FE mesh. The CA model simulates the development of the envelope of the grains in the liquid. For that purpose, a second FE mesh, referred to as CA mesh, is used. Fields can be interpolated between the adaptive FE mesh and the CA mesh. A CA grid made of a regular lattice of cubic cells is defined and superimposed onto the CA mesh. A new dynamic strategy for the allocation/deallocation of the CA grid is proposed to reduce the computation and memory costs. This CAFE model is applied to partial melting of an initial grain structure and epitaxial growth in the undercooled zone of a liquid pool, thus simulating the formation of solidification structure during the GTAW process. Examples of single linear passes simulations for various processing conditions and a multiple pass simulation are presented.

KEY WORDS: solidification; structures; welding; GTAW process; modeling.

1. Introduction

3D Cellular Automaton (CA) – Finite Element (FE) modeling is an efficient way to simulate the nucleation and growth of solidification grain structures in the context of casting processes.[1–3] This approach is usually known as CAFE modeling and has been widely used for the simulations of solid structures formed from the melt during casting processes.[4–6] Gandin and Rappaz[7] proposed the decentred octahedron CA growth algorithm to simulate the overall dendritic grain envelope in 3D. It was followed by a first dynamic allocation strategy[4] capable of handling large volume casting.[6] These algorithms have been recently improved by Carozzani and co-workers[8–11] to reach predictions for even larger casting size thanks to the use of parallel computing facilities and special dynamic allocation strategies.

While the above progresses were significant, they did not permit to handle simulations of the grain structure during welding process. This is due to the fact that the initial domain, named coupon, contains an initial grain structure that must be known at all locations and at any time in order to compute its local melting and the epitaxial growth from partially remelted grains, *i.e.* the solidification of the weld pool. So far, only few studies concern direct simulation of solidification structures for welding processes. For instance, Pavlyk *et al.*[12] simulated the dendritic grain growth under constrained solidification conditions typical for weld pool solidification. The temperature gradient and the solidification velocity in the weld pool were provided by a solution of the heat flow using the Finite Difference Method (FDM). Zhan *et al.*[13,14] developed the morphological evolution of columnar dendrites in the weld pool. The constitutional and curvature undercooling were considered in the computation of the solid-liquid interface velocity and provided by the FDM. Tan *et al.*[15] proposed a novel model that coupled CA and phase field to simulate the dendritic grain growth. The epitaxial growth was identified by defining both the grain density and dendrite arm density at the fusion line. In addition, Saluja *et al.*[16] applied a CAFE model to predict the grain size distribution and the influence of weld defects during friction stir welding. More work was achieved in the past in order to model the computation between grains, either with respect to crystal orientation[17–23] or to the columnar-to-equiaxed transition (CET).[23]

However, the works listed above focused on direct simulation of the growth of a few dendritic grains in representative solidification conditions of the weld pool, or on indirect modeling of the growth in the weld pool. No direct prediction of the final weld structure was proposed yet in 3D. The reason is due to the relative dimensions of the problem: the final weld structure in a coupon of industrial scales relevance is made of millions of grains, which was not targeted so far. Moreover, multiple pass welding that requires the possibility of several successive simulations and large domain computation were not reachable. A solution is presented in this paper that permits simulation of multiple passes in welding processes for large computational domains based on 3D CAFE modeling. In the first part, extensions of the CAFE model are detailed. In the second part, simu-

* Corresponding author: E-mail: Shijia.Chen@mines-paristech.fr
DOI: http://dx.doi.org/10.2355/isijinternational.54.401

lations are presented and discussed that illustrate single pass and multiple passes welding.

2. Modeling

2.1. FE Model

Ignoring the mechanical contributions in a parallelepipedic domain that represents a coupon submitted to a welding process, the energy conservation average over all phases can be established:[24]

$$\rho \frac{\partial \langle h \rangle}{\partial t} - \nabla \cdot \langle \kappa \nabla T \rangle = \dot{Q}_T \quad \text{..... (1)}$$

where ρ is the average mass density assumed uniform and constant for all phases, $\langle h \rangle$ is the average mass enthalpy, T is the temperature, $\langle \kappa \rangle$ is the average thermal conductivity and $\dot{Q}_T$ is a volumetric contribution of heat. In the present work, the energy conservation equation is solved in its enthalpy form using the FE method. Therefore, the equation yields the average mass enthalpy $\langle h \rangle$ as solution at each time step. It can be converted to the temperature as well as to the fraction of each solid or liquid phase by the following relations:

$$\langle h \rangle = \sum_{\alpha} f^{\alpha} \langle h^{\alpha} \rangle^{\alpha} \quad \text{..... (2)}$$

$$\langle h^{\alpha} \rangle^{\alpha} = \langle h^{\alpha} \rangle^{\alpha} \left(\langle w_i^{\alpha} \rangle^{\alpha}, T \right) \quad \text{..... (3)}$$

$$\langle w_i^{\alpha} \rangle^{\alpha} = \langle w_i^{\alpha} \rangle^{\alpha} \left(\langle w_i \rangle, T \right) \quad \text{..... (4)}$$

$$f^{\alpha} = f^{\alpha} \left(\langle w_i \rangle, T \right) \quad \text{..... (5)}$$

where $\langle h^{\alpha} \rangle^{\alpha}$, $\langle w_i^{\alpha} \rangle^{\alpha}$ and f^{α} are the intrinsic average mass enthalpy, the intrinsic average composition of component i and the mass fraction in phase α, respectively, and $\langle w_i \rangle$ is the average composition of component i. Thus the intrinsic average mass enthalpy of each phase $\langle h^{\alpha} \rangle^{\alpha}$ depends on its composition, $\langle w_i^{\alpha} \rangle^{\alpha}$, and the temperature, T, according to Eq. (3). Similarly, the composition of each phase, $\langle w_i^{\alpha} \rangle^{\alpha}$ and its mass fraction, $f^{\alpha} g^{\alpha}$, depends on the average composition of the material, $\langle w_i \rangle$ and the temperature, T according to Eqs. (4) and (5), respectively. The Gulliver-Scheil solidification path[26,27] is adopted in the present approach. Consequently, no solute diffusion occurs in the solid domains. The mass fraction and enthalpy of each phase are tabulated as illustrated in **Fig. 1** for alloy URANUS2202.[25] Tabulations are established thanks to the software Thermo-Calc[28] using the TCFE6 thermodynamic database.[29] Please note that, due to the Gulliver-Scheil approximation, several solid-state transformations are not accounted for, yet experimentally found in steels. Implementation of such paths can yet be considered using more advanced thermodynamic consideration, such as the partial and paraequilibrium.[31,32]

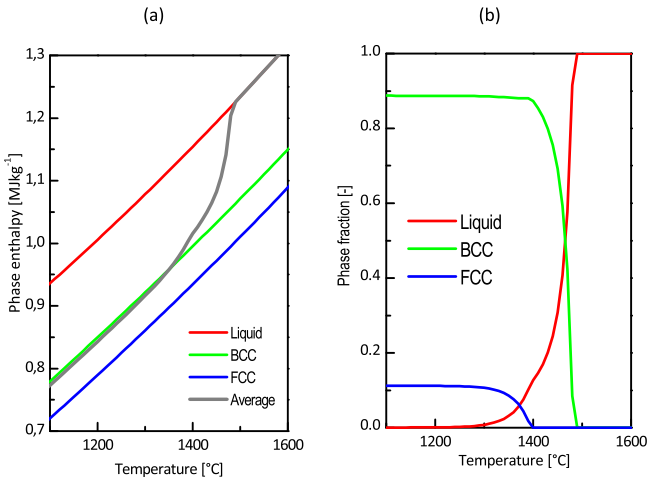

Fig. 1. Properties of the steel grade URANUS 2202[25] with chemical mass composition Fe–0.02C–22Cr–2Ni–2Mn–0.45Mo–0.2N showing (a) average phase enthalpy of phases liquid, BCC (ferrite) and FCC (austenite) and (b) mass fraction assuming the Gulliver-Scheil[26,27] solidification path. (Online version in color.)

2.2. CA Model

In the present work, the goal of the CA model is to simulate the grain structure in weld pools by changing the state indexes of the cells. According to Gandin *et al.*,[30] the branching mechanisms of dendrite arms and thus grain competition can be well reproduced when the cell size is smaller than the critical branching size. This means a typical cell size of the order of 50 to 100 μm is needed. In 3D simulations, it corresponds to 1 to 8 million cubic cells per cm^3. However, the intended resolution scale of the industrial welding model is in the magnitude of meter with a minimum representative domain given by the dimension of a typical coupon, *e.g.* 350 × 150 × 12 mm^3 corresponding to 0.63 to 5.04 billion cells. It would cost a lot of resources to resolve the CA model if all the cells of the coupon are allocated into the memory of the computer.

For modeling the solidification grain structure during welding processing, a very first and immediate reduction of the size of the problem can be achieved by considering a volume of the domain smaller for the CA method than for the FE method. This is done by considering two meshes, the FE mesh to solve the heat flow problem on the defined domain and the CA mesh to generate the CA grid and compute the grain structure on a reduced domain. The use of two meshes also permits to perform optimizations of the FE mesh for the heat flow computation, *i.e.* mesh adaptation, while the CA mesh can be kept fixed. The other advantage is the possibility to handle independent partitioning as already explained elsewhere.[9] However, communication between the two meshes then needs to be organized: following the CAFE coupling scheme,[8] the temperature field computed on the FE mesh must be projected onto the CA mesh for performing the algorithms of remelting and grain growth in later solidification on the CA grid. Oppositely, the fraction of liquid, growing and solid cells in the volume associated to the triangles defined for a given node of the CA mesh should be made available on the FE mesh to solve the heat flow problem.

Figure 2 gives an illustration of this simple optimization. For the sake of clarity, it is presented in a 2D approximation while all examples of calculations are later given in 3D. The figure presents two different domain sizes for the FE and CA meshes as well as a CA grid made of a regular lattice of square cells defined from the CA mesh. The triangular elements in FE and CA meshes and the square cells in CA grid are chosen large enough on purpose in order to be able to distinguish them in this illustrative example. In the present work, they are referred as FE elements, CA elements and

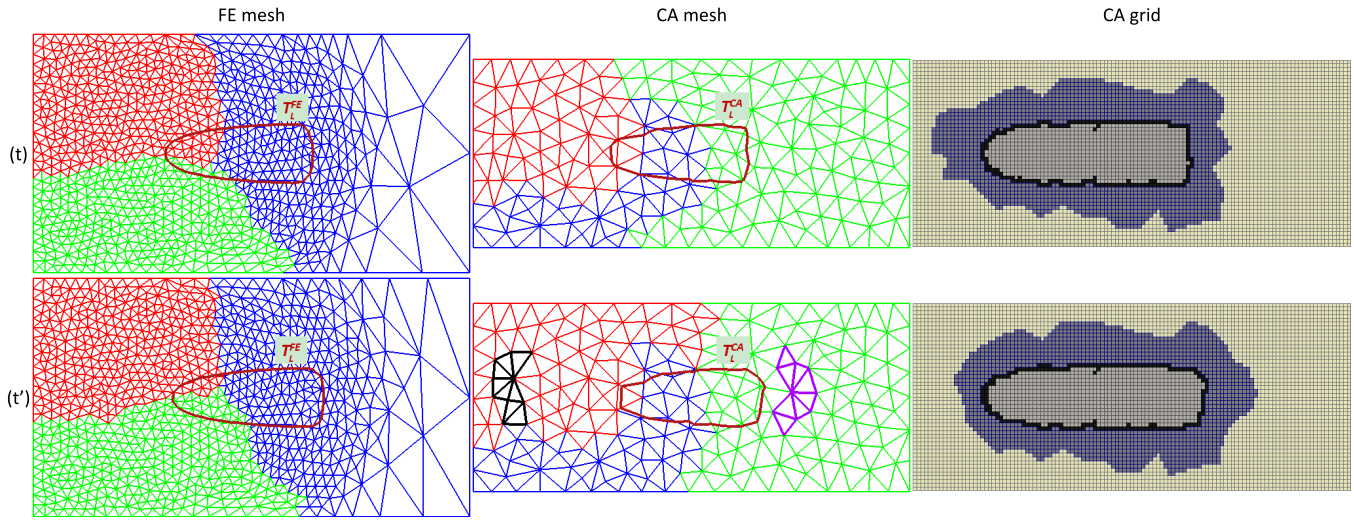

Fig. 2. 2D CAFE illustration of (FE mesh) FE mesh, (CA mesh) CA mesh and (CA grid) CA grid at (t) time t and (t′) time t′ > t. The domain sizes of FE and CA mesh are 350 × 190 mm^2 and 350 × 150 mm^2, respectively. CA grid made of a regular lattice of square cells is superimposed on CA mesh. The heat source moving at constant velocity from left to right between t and t′. The red, green and blue colors of the triangular meshes correspond to the partitions defined for parallel computations on 3 computational units. The square cells in CA grid are (light grey) liquid, (grey) not growing and (dark grey) growing (*i.e.* with at least one liquid neighboring cell). They are active and allocated in computer memory. The yellow cells are inactive and out of memory. The thick dark red contours identify (FE mesh) the position of the liquidus isotherm, T_L^{FE}, and (CA mesh) its projection onto the CA mesh, T_L^{CA}. The size of elements of the FE mesh, CA mesh and cells of CA grid are chosen very coarse on purpose for these illustrations. Triangular contours highlighted in black and purple in (CA-t′) correspond to activated and inactivated elements of CA mesh between times t and t′, respectively. (Online version in color.)

CA cells, respectively. The configuration of the simulation is a traveling heat source at constant velocity from left to right that locally heat and remelt the metal, later resolidified behind it. The information of the remelted zone is provided by the liquidus isotherm drawn as thick dark red contours. Note that, to be conducted, the change of the domain size requires knowing in advanced the size of the weld pool so as to make sure that it is fully included on the domain defined by the reduced CA mesh. As can be seen, the liquidus isotherms computed on the FE mesh, T_L^{FE}, and projected on the CA mesh, T_L^{CA}, differ. This is due to the different sizes of elements used on the FE and CA meshes, *i.e.* FE elements and CA elements. This illustration thus permits to identify the role of the size of the elements on the linear projection from a fine mesh to a coarse mesh. The opposite operation, *i.e.* projection from the coarse CA mesh to the fine FE mesh, does not lead to such loose of information. One can also see by comparing Figs. 2(t) and 2(t′) that the T_L^{CA} contour changes with time while the T_L^{FE} contour remains stable, *i.e.* is simply translated due to the heat source move in stationary conditions. This is reached thanks to the mesh adaptation of the FE mesh, not achieved with the fixed CA mesh.

Under welding processing, the coupon is at low temperature before being heated and melted by a heat source. Therefore, the initial solid structure is required before calculation. The initial solid structure, usually equiaxed, is deduced from a first CAFE simulation of the structure formed during casting assuming nucleation and growth of grains in a uniform temperature domain.[8] The final casting structure is consequently equiaxed. It serves as the initial welding structure and is stored on a hard disk as a set of files. In order to satisfy the allocation scheme that will be presented hereafter, each file corresponds to a specific CA element. Because the CA mesh is fixed, each file can be uniquely linked to the barycentric coordinates of the corresponding CA element. Note that other initial structures could be considered, for instance with an initial texture and elongation that would result from a rolling process of the coupon. Because the present structure is fully equiaxed, grains have an isotropic shape and no preferred crystallographic orientation with respect to the axes of the simulation domain.

The procedures to activate/deactivate the CA elements and the CA cells are now presented below. The model considers that the initial structure does not evolve if it is not heated to the liquidus temperature. This means that morphological evolution such as solid-state grain growth is not taken into account. During welding, a specific CA element will be activated when at least one of the conditions below is fulfilled

- at least one node of the element is above the liquidus temperature,
- at least one of its neighboring element fulfills the previous condition.

The second condition is necessary in the present dynamic allocation algorithm because the fraction of growing cells of a specific node in the CA mesh is dependent on all the cells in the CA elements connected to this node. When a CA element is activated, the corresponding file containing the cell information will be read and then removed from the hard disk. These cells are considered in the CA resolution until the corresponding CA element is deactivated, which occurs when both the conditions below are fulfilled simultaneously:

- all the nodes of the element are below the liquidus temperature,
- the fraction of growing cells of all the nodes of the element is equal to 1.

The information associated to the cells belonging to the CA element is then written into a file linked to its barycen-

tric coordinates and stored on the hard disk. It can thus be read again when/if the heat source heats sufficient the same element, for instance in case of multiple passes.

The cells are allocated in an active CA element, *i.e.* they retrieve the solid state index in which they were stored and change their state indexes with respect to their local temperatures and neighborhood states:

- if a cell is above the liquidus temperature, it adopts the state index of a liquid cell,
- if it is below the liquidus temperature but has at least one neighboring cell in the liquid state, its state index is changed to a growing cell. The grain information of its previous state is then also created.

It can be deduced from the above procedures that cells cannot be created individually. Instead, all cells of a CA element are read/stored on the corresponding file. Therefore, the dynamic allocation/deallocation of the CA cells is reduced to the dynamical activation/deactivation of the CA elements.

Figures 2(CA mesh-t′) and 2(CA grid-t′) are also used to illustrate the above listed activation/deactivation and allocation/deallocation procedures. When time increases from t to t′ > t, the liquidus isotherm is moved to the right-hand-side. Consequently, in Fig. 2(CA mesh-t′), the 8 elements highlighted in purple fulfill the activation conditions and are thus activated. The 8 corresponding files with cell information are read and stored into the computer memory prior to be removed from the hard disk, thus allocating the corresponding CA cells defined by these 8 elements, which is shown in Fig. 2(CA grid-t′), *i.e.* the corresponding cells are changed from inactive states (yellow color) to active but not growing states (grey color). During the same period of time, the 8 elements highlighted in black fulfill the deactivation conditions and thus are deactivated. The cell information of each element is then written into 8 corresponding files and the memory is released of the corresponding CA cells information. Note that the numbers of activated/deactivated elements are independent to each other. In the CA elements that experience a temperature increase above the liquidus temperature between time t and t′, the cells located inside the liquidus isotherm contour are changed to liquid state. This is made visible in Fig. 2(CA mesh-t′) by considering all cells that have changed color to become light grey between time t and t′. The cells located outside the liquidus isotherm but with liquid neighborhood are changed to mushy state, *i.e.* to the dark grey color. The grey cells are below the liquidus temperature and far enough from the growing structure to have no liquid neighboring cell.

In Fig. 2, additional information is provided by the FE and CA meshes considering the 3 colors of the elements edges. It corresponds to the partition of the calculation on 3 computing units. As can be seen, partitioning is such that the number of nodes per computing unit is approximately the same. For the CA mesh, partitioning is based on an even distribution of the active CA cells among the 3 computing units.[9)]

3. Simulation Results and Discussions

The first application of the present CAFE model with extended procedure for welding processes is intended to simulate single linear pass upon Gas Tungsten Arc Welding (GTAW) for various welding parameters in URANUS 2202 (**Table 1** and Fig. 1). The parameters of initial and boundary conditions are also listed in Table 1. For the grain growth kinetic law in Table 1 particularly, the parameters A and n used here are approximated but representative values. Better values could be deduced by fitting a computed KGT solution.[33)] The Goldak volumetric heat source[34)] is adopted. The ellipsoidal power density distribution of the heat source is given by the following relationship:

$$q(x.y,z,t) = \frac{6\sqrt{3}Q}{abc\pi\sqrt{\pi}} e^{-3(x-vt)^2/c^2} e^{-3y^2/a^2} e^{-3z^2/b^2} \quad \text{.... (6)}$$

where Q is the input power, v is the velocity of the heat source, a, b and c are semi-axes of the ellipsoidal heat source in the Y, Z and X directions, respectively. The values of these parameters are listed in **Table 2** for 4 different simulations presented hereafter. Note that only Q and v have been changed, all starting points (X_S, Y_S, Z_S) and ending points (X_E, Y_E, Z_E) defining the trajectory of the heat source being kept constant. The numerical parameters of the calculations are given in **Table 3**.

Table 1. Material parameters for URANUS 2202 and boundary conditions for the simulations.

Parameter	Symbol	Value
Heat transfer coeff. ($Wm^{-2}K^{-1}$)	h	5
Emissivity (–)	e	0.25
Initial temperature (°C)	T_0	20
External temperature (°C)	T_{ext}	20
Liquidus temperature (°C)	T_L	1 481
Initial grain density (m^{-3})	N_0	10^{11}
Grain growth kinetics (ms^{-1}) $v_{CA} = A\,\Delta T^n$	A	10^{-7}
	n	2.0

Table 2. Parameters of the Goldak volumetric heat source for the simulations.

Parameters	Single linear pass GTAW				Multi-pass GTAW		
	(1)	(2)	(3)	(4)	P1	P2	P3
v (mm s^{-1})	1	1.5	5	1.5		4	
Q (W)	5 000	7 500	15 000	5 000	25 000	18 000	15 000
X_S, Y_S, Z_S (mm)	75, 75, 12				20,15,50	20,17,50	20,13,50
X_E, Y_E, Z_E (mm)	275, 75, 12				100,15,50	100,17,50	100,13,50
a (mm)	18				3	3	3
b (mm)	10				60	50	45
c (mm)	18				3	3	3

Table 3. Numerical parameters for the two GTAW simulations.

Parameter	Single pass	Multiple passes
FE domain (mm^3)	350 × 150 × 12	120 × 30 × 50
Initial FE mesh size (mm)	5	3
Number of FE nodes (–)	10 000	10 000
CA domain (mm^3)	240 × 30 × 12	120 × 30 × 50
CA element size (fixed) (mm)	3	3
CA cell size (μm)	80	80
Number of processors (–)	32	64

The 3D CAFE grain structures of single pass GTAW are presented in **Fig. 3** as predicted on the top surface on the domain and in a transverse cross section. Because the initial structure is fully equiaxed with a very small size due to the high initial grain density N_0 and the regrown structure is columnar with an elongated shape factor, it is easy to recognize the region where remelting and resolidification took place. The width and depth of the pool are thus found to vary with the processing conditions. The weld pool is found to decrease when the velocity of the heat source is increased, *i.e.* cases (1) at 1 mm s^{-1} and (4) at 1.5 mm s^{-1}, and when the input power of the heat source is decreased, *i.e.* cases (2) at 7 500 W and (4) at 5 000 W. For low velocity (1) and/or low power (4), the growth direction of the grains tends to follow the path of the heat source. Some grains can indeed even survive columnar competition at the center of the weld and grow over a very long distance before they are stopped. The reason is that the temperature gradient remains low so that grain competition is not highly pronounced according to the grain growth kinetics law in Table 1. In comparison, competition taking place among the columnar grains predicted for a strong increase of the power is such that no long

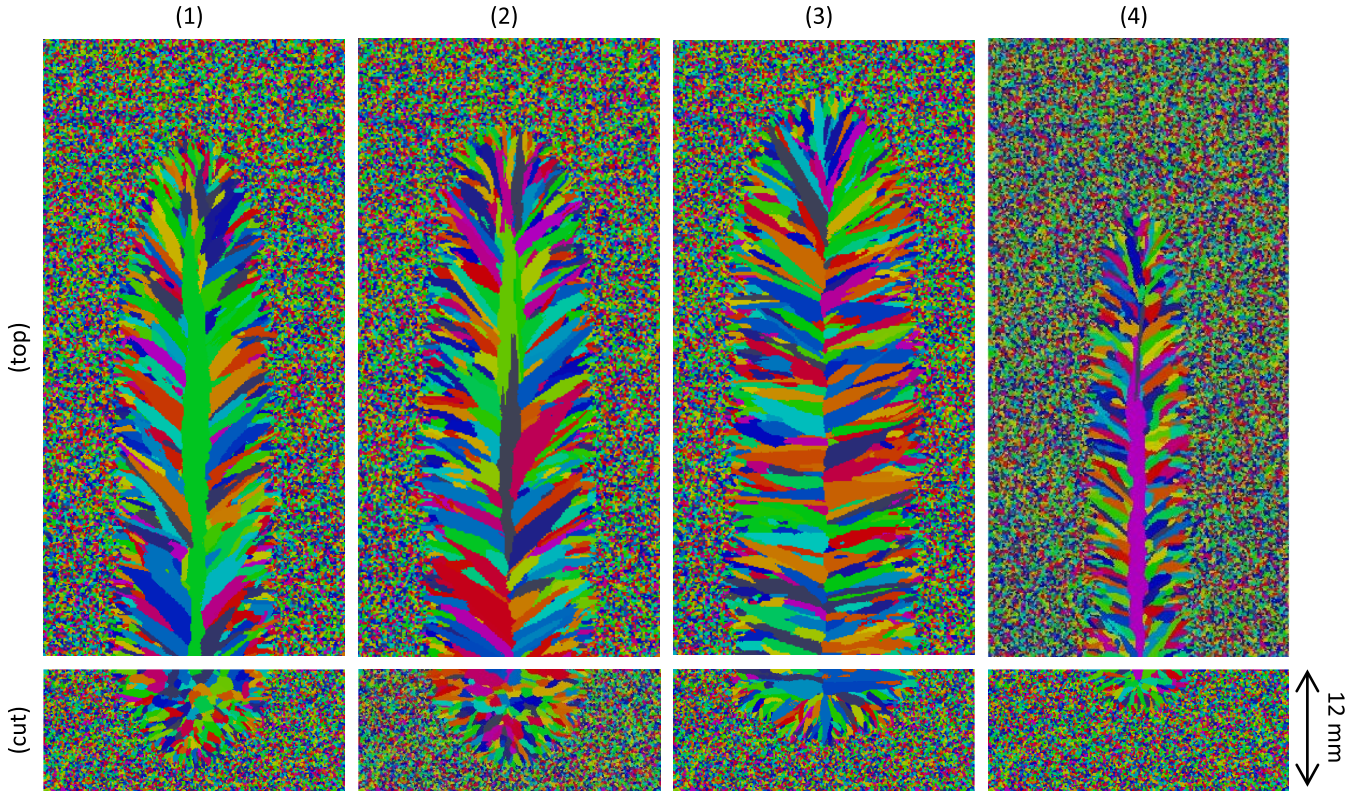

Fig. 3. Simulated 3D CAFE grain structures for four single linear GTAW passes (top) as observed from the top surface of the domain in the range 70 mm < X < 130 mm and (cut) in a transverse cross section at coordinate X = 130 mm. Heat source parameters and velocity corresponding to cases (1) to (4) are reported in Table 2. Material parameters and numerical parameters are given in Tables 1 and 3, respectively. (Online version in color.)

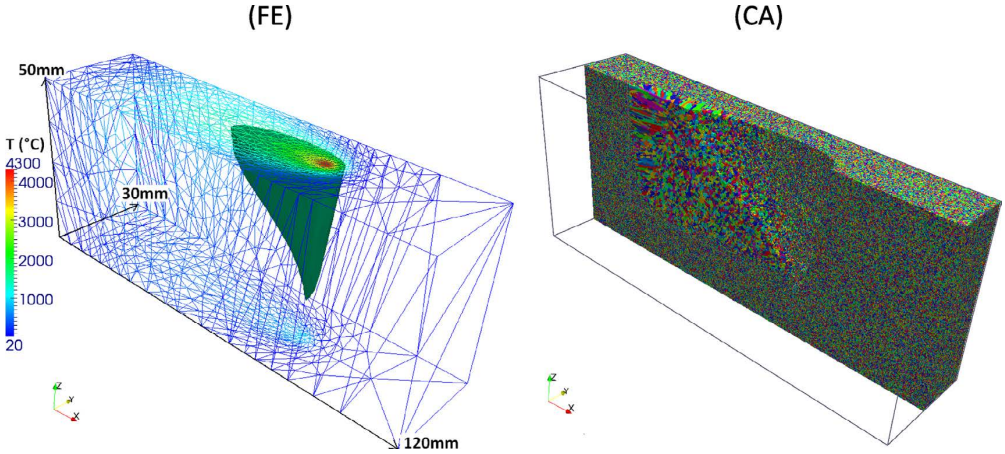

Fig. 4. Snapshot at 32.5 s during the first pass of the 3D CAFE grain structure simulation for the multiple passes GTAW showing (FE) the FE mesh on the sides of the domain (colors are proportional to the temperature) and (CA) the grain structure in half the volume of the domain as well as the mushy zone – liquid boundary where the grain envelops grow into the liquid. The liquidus isotherm computed on the refined FE mesh is represented by the red contour in (FE). Parameters are accessible in Tables 1–2. (Online version in color.)

grains survive and that they are aligned with the source path. The grains are then more directed toward the centerline of the weld. This is even more pronounced at very high velocity in Fig. 3(3). Overall, these results retrieve common trends expected in solidification structure formed during welding as can be read in standard physical metallurgy textbooks.[35] It also provides with a 3D extension of previous 2D attempts to model welding structures with a CAFE model.[36]

The predictions upon multiple passes permit better understanding of the improvement achieved with the present 3D CAFE model. Three successive linear passes are defined by the parameters given in Table 2. The starting and ending points of the heat source are such that overlapping of the weld pools can take place, the first pass taking place at the center of the top XY plane of the domain and the second and third passes taking place on its side with a +2 mm and –2 mm shift in the Y directions, respectively. Prior to consider the final result of the several passes, it is interesting to consider the temperature field given in **Fig. 4**(FE) at a given time during the first pass. The hot temperature spot at the top surface of the domain indicates the position of the heat source. The mesh size is the finest in its vicinity since it is adapted to track the regions of large temperature gradient. The 3D green contour according to the temperature scale represents the shape of the liquidus isotherm. It is well retrieved in Fig. 4(CA) when considering a cross section through the domain. Because the liquid cells are not represented, the shape of the weld pool can be directly visualized. It closely follows the shape of the isotherm where remelting takes place but departs from it where growth proceeds. The reason is due to the undercooling of the growing structure that develops the growth front below the liquidus isotherm. Fig. 4(CA) also reveals the growth competition taking place upon columnar growth and epitaxial growth of the equiaxed

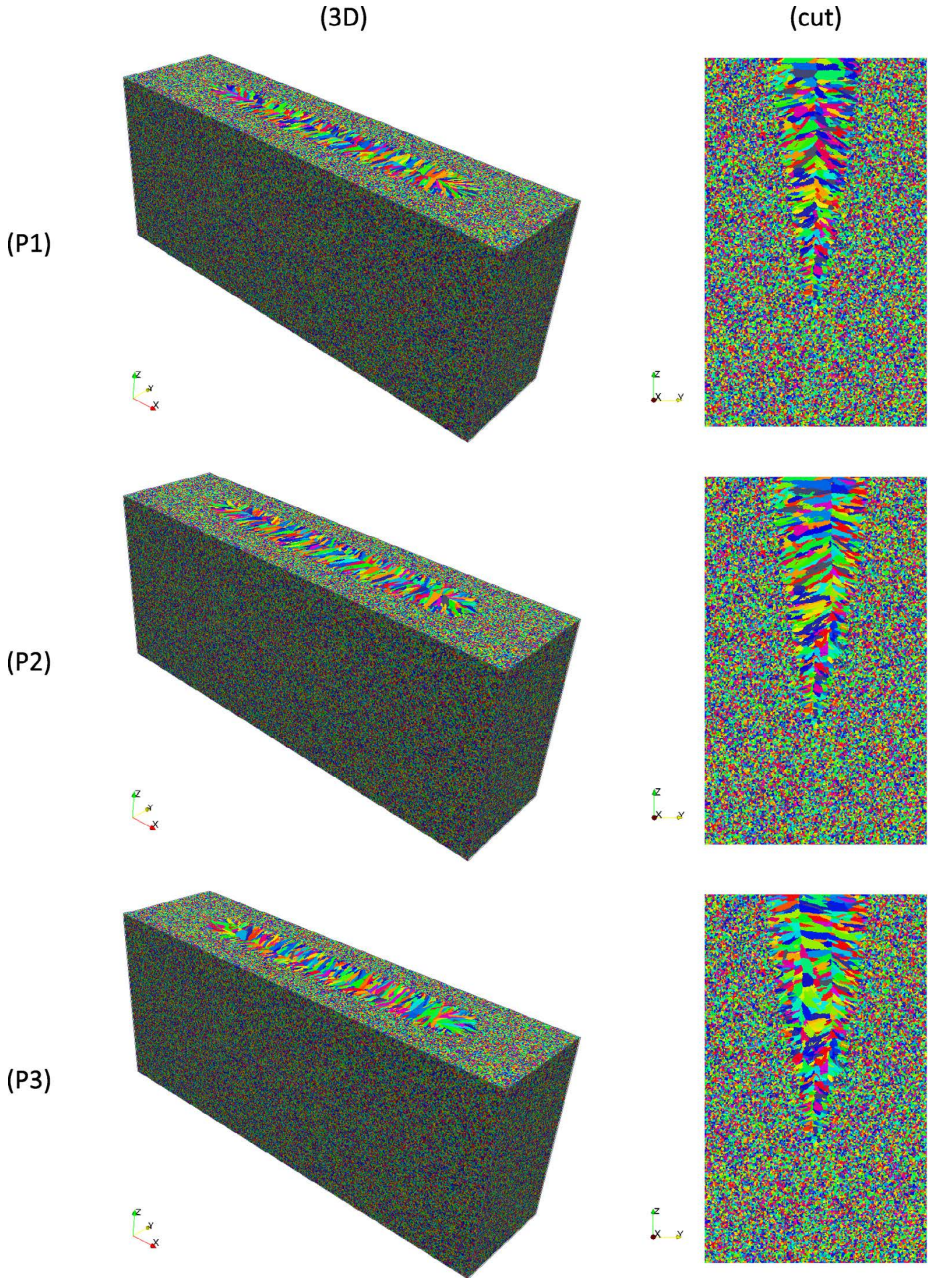

Fig. 5. 3D CAFE grain structures of the multiple passes GTAW simulation shown in Fig. 4 observed (3D) at the boundaries of the domain and (cut) in a transverse cross section at coordinate X = 60 mm at the end of (P1) path 1, (P2) path 2, (P3) path 3. Parameters are accessible in Tables 1–2. (Online version in color.)

grains that are partly melted. Note that in all simulations it was assumed no nucleation of equiaxed grains in the pool, as is sometime observed in the literature.[35] It would have been possible to handle such nucleation as demonstrated in other 3D CAFE simulations.[8]

Figure 5 presents the final structure after each of the 3 passes, with the same view as in Fig. 4 but also in a transverse cross section. After the first pass, the columnar grains are found to meet at a symmetrical surface defined by the heat source path. Because the second pass is shifted to the right-hand-side, the columnar grains now form a meeting line also shifted to the right as seen in Fig. 5(P2-cut). The initial columnar grain structure seen on the right-hand-side of Fig. 5(P1-cut) was fully remelted up to the lower depth reached by the weld pool. In fact, the weld pool input power was decreased as shown in Table 2. But only part of the left-hand-side columnar structure of Fig. 5(P1-cut) was melted so epitaxial growth could take place on the already existing columnar grains, resulting in the dissymmetry of the structure seen in Fig. 5(P2-cut). Finally, upon pass 3 operated 2 mm on the left-hand-side of pass 1, namely 4 mm left of pass 2, the structure generated during the second pass is only partially remelted and propagated. A second line appears in the structure. The cross section in Fig. 5(P3-cut) reveals evidence of the 3 successive passes with a very complicated final grain structure.

4. Conclusions and Perspectives

A two meshes strategy with dynamic activation/deactivation of CA elements and allocation/deallocation of CA cells is presented for modeling of grain structure formed during welding processing with a 3D CAFE model. The cells data is stored in hard disk by a set of files corresponding to the CA elements. Only the cells associated to the growing front are allocated and considered in the CA resolutions. They are deallocated and stored onto the hard disk when the structure is fully developed.

The implementations of present CAFE model is shown to successfully predict the grain structure considering only remleting and resolidification upon single linear pass and multiple overlapping linear passes during GTAW, *i.e.* with no metal addition. It is shown that the heat source velocity and power largely modifies the grain structure as a result of its influence on the temperature field.

For the first time direct simulation of 3D grain structures in large domains are presented for a welding process. Several studies can already be conducted with the model that were not possible in the past: oriented-to-misoriented and columnar-to-equiaxed transitions,[23] competition between <100> directions observed upon remelting of a single crystal,[20] structures formed upon multiple passes during GTAW.[21,22] It is yet clear that such model is not necessarily restricted to remelting processes. However, extension to processing that permits addition of metals still requires extensions. Current developments consist of level set tracking of the metal-air interface, with possible increase of the metal domain due to deposit of melted droplets. This requires considering a CA grid in the air with transition from metal cell to air cell, thus further extending to several phases the cell information. Finally, grain structure evolution in the heat affected zone could also be the subject of investigations with the CA method. Another extension of relevance for welding processing is the coupling with thermomechanical deformations.

Acknowledgements

This work is funded by ARMINES and China Scholarship Council (CSC) (grant 2010623175).

REFERENCES

1) Ch.-A. Gandin, M. Rappaz and R. Tintillier: *Metall. Trans. A*, **24** (1993), 467.
2) Ch.-A. Gandin, M. Rappaz and R. Tintillier: *Metall. Trans. A*, **25** (1994), 629.
3) Ch.-A. Gandin, M. Rappaz, D. West and B. L. Adams: *Metall. Trans. A*, **26** (1995), 1543.
4) Ch.-A. Gandin, J.-L. Desbiolles, M. Rappaz and Ph. Thévoz: *Metall. Mater. Trans. A*, **30** (1999), 3153.
5) H. Takatani, Ch.-A. Gandin and M. Rappaz: *Acta Mater.*, **48** (2000), 675.
6) P. Carter, D. C. Cox, Ch.-A. Gandin and R. C. Reed: *Mater. Sci. Eng. A*, **280** (2000), 233.
7) Ch.-A. Gandin and M. Rappaz: *Acta Metall. Mater.*, **45** (1997), 2187.
8) T. Carozzani, H. Digonnet and Ch.-A. Gandin: *Model. Simul. Mater. Sci. Eng.*, **20** (2012), 015010.
9) T. Carozzani, Ch.-A. Gandin, H. Digonnet, M. Bellet, K. Zaidat and Y. Fautrelle: *Metall. Mater. Trans. A*, **44** (2013), 873.
10) T. Carozzani, Ch.-A. Gandin and H. Digonnet: *Model. Simul. Mater. Sci. Eng.*, **22** (2014), 015012.
11) Ch.-A. Gandin, T. Carozzani, H. Digonnet, S. Chen and G. Guillemot: *JOM*, (2013), DOI 10.1007/s11837-013-0679-z.
12) V. Pavlyk and U. Dilthey: *Model. Simul. Mater. Sci. Eng.*, **12** (2004), S33.
13) X. H. Zhan, Z. B. Dong, Y. H. Wei and Y. L. Xu: *Cryst. Res. Technol.*, **43** (2008), 253.
14) X. H. Zhan, Z. B. Dong, Y. H. Wei and R. Ma: *J. Cryst. Growth*, **311** (2009), 4778.
15) W. Tan, N. S. Bailey and Y. C. Shin: *J. Manuf. Sci. E.-T. ASME*, **134** (2012), DOI 10.1115/1.4007101.
16) R. S. Saluja, R. G. Narayanan and S. Das: *Comp. Mater. Sci.*, **58** (2012), 87.
17) M. Rappaz, S. A. David, J. M. Vitek and L. A. Boatner: *Metall. Trans. A*, **20** (1989), 1125.
18) S. A. David, J. M. Vitek, M. Rappaz and L. A. Boatner: *Metall. Trans. A*, **21** (1990), 1753.
19) M. Rappaz, S. A. David, J. M. Vitek and L. A. Boatner: *Metall. Trans. A*, **20** (1990), 1767.
20) M. Rappaz, J. M. Vitek, S. A. David and L. A. Boatner: *Metall. Trans. A*, **24** (1993), 1433.
21) J. Moysan, A. Apfel, G. Corneloup and B. Chassignole: *Int. J. Press. Ves. Pip.*, **80** (2003), 77.
22) A. Apfel, J. Moysan, G. Corneloup, T. Fouquet and B. Chassignole: *Ultrasonics*, **43** (2005), 447.
23) S. Mokadem, C. Bezençon, A. Hauert, A. Jacot and W. Kurz: *Metall. Mater. Trans. A*, **38** (2007), 1500.
24) M. Rappaz, M. Bellet and M. Deville: Numerical Modeling in Materials Science and Engineering, Springer, Berlin, (2003).
25) Arcelor Mittal: URANUS2202 Rev.7, http://www.industeel.info/datasheets/pdf/ur2202.pdf. (2010).
26) G. M. Gulliver: *J. Inst. Met.*, **9** (1913), 120.
27) E. Scheil: *Z. Metallkd.*, **34** (1942), 70.
28) Thermo-Calc, TCCS Manuals, Thermo-Calc software AB, Stockholm, SE, (2013).
29) P. Shi: TCS Steels/Fe-alloys Database, V6.0, Thermo-Calc Software AB, Stockholm, SE, (2008).
30) Ch.-A. Gandin and M. Rappaz: *Acta Metall. Mater.*, **42** (1994), 2233.
31) H. Zhang, K. Nakajima, Ch.-A. Gandin and J. He: *ISIJ Int.*, **53** (2013), 493.
32) T. Koshikawa, Ch.-A. Gandin, M. Bellet, H. Yamamura and M. Bobadilla: *ISIJ Int.*, (2014), submitted.
33) W. Kurz, B. Giovanola and R. Trivedi: *Acta Metall.*, **34** (1986), 823.
34) J. Goldak, A. Chakravarti and M. Bibby: *Metall. Trans. B*, **15** (1984), 299.
35) D. A. Porter and K. E. Easterling: Phase Transformations in Metals and Alloys, 2nd ed. Chapman&Hall, London, (1992), 245.
36) M. Rappaz, Ch.-A. Gandin, J.-L. Desbiolles and Ph. Thévoz: *Metall. Mater. Trans. A*, **27** (1996), 695.